The properties of highly concentrated aqueous CH_3COOK/Na binary electrolyte and its use in sodium-ion batteries

*Shahid Khalid[a], Nicolò Pianta[a], Simone Bonizzoni[a], Piercarlo Mustarelli[a,b], Riccardo Ruffo[a,b]**

[a]Department of Materials Science, University of Milan-Bicocca, via Cozzi 55, 20125, Milan, Italy

[b]National Reference Center for Electrochemical Energy Storage (GISEL) - Consorzio Interuniversitario Nazionale per la Scienza e Tecnologia dei Materiali (INSTM), 50121 Firenze, Italy

KEYWORDS: Water in salt, aqueous electrolytes, sodium ion batteries, NASICON, electrochemical stability window,

ABSTRACT

Highly concentrated aqueous binary solutions of acetate salts are emerging as promising systems for advanced energy storage applications. Together with superior solubility of CH_3COOK helpful in achieving water-in-salt electrolyte concentrations, the presence of CH_3COOLi or CH_3COONa permits intercalation of desired cations in electrode crystalline phases. Although these systems

have captured profound scientific attention in recent years, a fundamental understanding of their physicochemical properties is still lacking. In this work, the thermal, rheological, transport, and electrochemical properties for a series of solutions comprising of 20 mol kg^{-1} of CH_3COOK with different concentrations of CH_3COONa are reported and discussed. The most concentrated solution, i.e., 20 mol kg^{-1} of CH_3COOK with 7 mol kg^{-1} of CH_3COONa came out to be the best in terms of a compromise between transport properties and electrochemical stability window. Such a solution has a conductivity of 21.2 mS cm^{-1} at 25°C and shows a stability window up to 3 V in "ideal" conditions, i.e., using small surface area and highly electrocatalytic electrode in a flooded cell. As a proof of concept of using this solution in sodium-ion batteries, carbon-coated $LiTi_2(PO_4)_3$ (NASICON) demonstrated the ability to reversibly insert and de-insert Na^+ ions at about -0.7 V vs. SHE with a first cycle anodic capacity of 85 mAh g^{-1}, average charge efficiency of 96% at low current and a 90% capacity retention after 60 cycles. The very good kinetic properties of the interface are also demonstrated by the low value of activation energy for the charge transfer process (0.12 eV).

Introduction

Driven by the unique benefits of inherent safety, low cost, electrochemical stability, high ionic conductivity and environmental friendliness, super-concentrated aqueous electrolytes are receiving great interest in defining new chemistries for batteries [1]. Although conventional lithium-ion batteries (LIBs) employing organic electrolytes have reached an acceptable performance limit, they still suffer of serious issues, such as safety and cost. The non-aqueous organic carbonate electrolytes used in conventional Li-ion batteries, indeed, have low flashpoints, high melting points and high viscosities rendering them useless at lower temperatures [2]. Moreover, conventional Li-ion batteries mostly rely on thermally unstable $LiPF_6$ which, in the presence of moisture, can

undergo degradation, giving HF and causing corrosion of battery components [3]. To alleviate these challenges, several strategies were proposed, including the use of non-flammable, less toxic and cost-effective aqueous electrolytes. However, a major limitation in the use of aqueous electrolytes is the extremely narrow thermodynamic electrochemical stability window (ESW) of water (1.23 V). Though the ESW can be kinetically extended up to 1.5 V using diluted salt solutions, such aqueous systems cannot yet compete with their organic counterparts, which translates into poor energy density [4].

To widen the ESW of aqueous electrolytes, researchers ventured into high concentration regimes, that were first discouraged by increased ion coupling and rheological limitations. As early as in 1985, McKinnon and Dahn reported a saturated $LiAsF_6$ solution in propylene carbonate (PC) demonstrating an unusual intercalation behavior that could not be possible in ordinary 1 M electrolyte [5]. Curiously, the earlier attempts to breach the concentration restraint were performed with polymer electrolytes, giving origin to the "Polymer-in-Salt" concept[6]. The extreme extension of super-concentration is the so-called "Water-in-Salt" electrolyte (WISE) developed by Suo et al., by dissolving LiTFSI in water up to 21 mol kg^{-1}, enabling a voltage window of 3 V [1,7]. The reason for this enhanced ESW stems from the low activity of water molecules at such a high concentration, where the ions outnumber the water molecules which are incorporated into the solvation shells [8]. In the high concentrated scenario, water molecules form clusters, in the sub-nanometer range, strongly interacting with one or more ions, resulting in large kinetic overpotentials for the electrolysis of water [9]. Wider ESW electrolytes employ per-fluorinated sulfonyl imide salts such as lithium (fluorosulfonyl)(trifluoromethane sulfonyl)imide (FTFSI) [10], lithium (pentafluoroethane sulfonyl)(trifluoromethane sulfonyl)imide (PTFSI), lithium

bis(trifluoromethanesulfonyl)imide (LiTFSI) [11], sodium trifluoromethanesulfonate (NaOTF) [12], sodium bis(fluorosulfonyl)imide (NaFSI) [13] and potassium trifluoromethanesulfonate (KOTF) [14].

Despite the outstanding improvements in the ESW, the environmental and economic concerns related to the use of fluorinated salts remain unresolved. In particular, LiTFSI, which is widely used in LIBs, exhibits severe oral and dermal toxicity, skin issues and can cause chronic aquatic toxicity [8]. Furthermore, the limited availability and very high cost of these fluorinated salts practically nullify the advantages brought by super-concentration, making the practical implementation of WISE in energy storage very challenging [15,16]. Conversely, the main problem in selecting new formulations for WISE is the lack of suitable salts with enough solubility to satisfy the WISE condition. Examples of cost-effective, highly soluble, and widely available salts are LiCl, CH_3COONa (NaAc), and CH_3COOK (KAc). In particular, KAc has been recently investigated by our group [17], proposed in potassium ion batteries (KIBs), and employed in supercapacitors [18]. Moreover, KAc can be coupled with Li, Na and Zn salts to achieve binary electrolytes with concentrations above 20 mol kg^{-1} [19]. For instance, S.G. Chen et al. reported a mixed-cation electrolyte composed of 32 mol kg^{-1} KAc and 1 mol kg^{-1} $(CH_3COO)_2Zn$ allowing a (2.0 V) Zn-MnO_2 aqueous rechargeable cell [20]. Another interesting report features a 32 mol kg^{-1} KAc with 7 mol kg^{-1} CH_3COOLi electrolyte utilizing C-TiO_2 an anode and $LiMnO_4$ as a cathode [8].

In the design of secondary batteries, a critical issue is the choice of electrode materials to be used in such a highly concentrated environment. In this framework, NASICON compounds offer significant advantages owing to their stable structure and large ionic channels with accessible sites for highly efficient ions insertion-extraction [21]. Moreover, the very low solubility and the possibility to modify the intercalation potential by tuning the chemical composition, so matching

the cell voltage with the electrolyte ESW, make NASICON compounds an ideal choice as electrode materials [18].

Taking advantage of the high solubility of KAc, we investigated a binary system comprised of KAc and NaAc, by keeping the KAc concentration constant at 20 mol kg^{-1}, and increasing NaAc up to 7 mol kg^{-1}. A single composition (32 mol kg^{-1} KAc with 8 mol kg^{-1} NaAc) was recently investigated as far as the electrochemical applications were concerned [22]. In this paper, we performed a careful study on the physico-chemical properties of the binary system, which are crucial to correctly address its application in batteries. To prove the advantages of using the most concentrated solution i.e., 7 mol kg^{-1} NaAc with 20 mol kg^{-1} KAc as a WISE electrolyte, we studied the intercalation process of alkaline ions (Na, K) using carbon-coated $LiTi_2(PO_4)_3$ NASICON as an electrode material. Such a material has already been used as the negative electrode with aqueous electrolytes[23]. The electrochemical measurements include a kinetic analysis trough impedance spectroscopy as a function of the temperature.

Experimental Section

Electrolyte preparation

Appropriate amounts of NaAc (99%, Alfa Aesar) and KAc (99%, Alfa Aesar) were dissolved in high-quality Milli-Q water (σ = 6.7 μS cm^{-1}) under sonication. Keeping KAc constant at 20 mol kg^{-1} and varying the concentration of NaAc, four different electrolytes were prepared, namely 1 mol kg^{-1} NaAc with 20 mol kg^{-1} KAc (1N20K), 2.5 mol kg^{-1} NaAc with 20 mol kg^{-1} KAc (2.5N20K), 5 mol kg^{-1} NaAc with 20 mol kg^{-1} KAc (5N20K), and 7 mol kg^{-1} NaAc with 20 mol kg^{-1} KAc (7N20K). 1 M NaAc solution was also prepared for comparison. All the electrolytes were stored and used at room conditions. The investigated samples are listed in Table 1 with the corresponding compositional parameters.

Materials Synthesis

Synthesis of CLTP

Carbon-coated $LiTi_2(PO_4)_3$ NASICON, (CLTP) phase was synthesized using a facile one-pot synthesis route. Firstly, 1.78 g of $NH_4H_2(PO_4)_3$ as a phosphate precursor were dissolved in 40 ml of ethanol via stirring, then 3.51 g of $Ti(OC_4H_9)_4$ as a Ti source were added until complete dissolution. As lithium and carbon sources, $CH_3COOLi{\cdot}2H_2O$, 0.52 g and $C_6H_{12}O_6$, 0.58 g were added, respectively. The mixture was stirred for 4 h at 55 °C in a sealed container. The system was then opened, and the temperature was raised to 80 °C to get rid of ethanol and obtain a gel. The precursor was dried under vacuum at 100 °C and finely grinded with mortar and pestle. The obtained powdered precursor was calcined at 800 °C for 6 h under argon flux in a tubular furnace. The ramp rate was set to 5 °C min^{-1} and the gas flow was adjusted to 50 ml min^{-1}. Pristine $LiTi_2(PO_4)_3$ (LTP) was synthesized via the same route, without using $C_6H_{12}O_6$ in the synthesis steps.

Table 1. Composition of NaAc/KAc/H_2O solutions

Sample Name	Density ($g{\cdot}cm^{-3}$)	Molarity ($mol{\cdot}dm^{-3}$)	Mol NaAc (%)	Mol KAc (%)	Mol H_2O (%)	Wt NaAc (%)	Wt KAc (%)	Wt H_2O (%)	n*
1N20K	1.37	9.45	1.31	26.14	72.55	2.69	64.47	32.84	2.64
2.5N20K	1.39	9.87	3.20	25.64	71.16	6.48	61.96	31.56	2.46
5N20K	1.40	10.38	6.20	24.84	68.96	12.16	58.19	29.65	2.22
7N20K	1.41	10.76	8.48	24.24	67.28	16.23	55.50	28.27	2.05
n*= ratio of the number of water molecules to the salt molecules									

Structural and Morphological Studies

X-Rays Diffraction analysis was carried out using Rigaku Miniflex 600 equipped with a Cu cathode. The analysis was performed in a 2θ range from 10° to 80° degrees with a step size of 0.02 and scan speed of 1 deg min^{-1}. Scanning electron microscopy (SEM) was done using Zeiss® Gemini SEM 450.

Viscosity Measurements

Viscosity measurements were done with MCR Rheometer 102 (Anthon Paar). A parallel plate (50 mm) setup was used to perform shear tests with shear rates in the range 10-300 s^{-1} with steady-state settings. The measurements were carried out at 10 °C, 20 °C, 30 °C and 40 °C.

Thermal Studies

Thermal analysis was performed with Differential Scanning Calorimetry (DSC) using DSC 1 Star® (Mettler Toledo). STARe® software was used for the evaluation of the data. The samples were analyzed in a temperature range from -120 °C to 90 °C. The following protocol was used: cooling from 30 °C to -120 °C at a rate of 1 °C min^{-1}, followed by a 5 min isotherm at -120 °C, and finally by a heating step from -120 °C to 90 °C at a ramp rate of 1 °C min^{-1}. Initially, all the samples were equilibrated at 30 °C for 30 minutes to ensure a completely liquid state. The heating/cooling rate of 1 °C min was chosen to allow the system to undergo structural relaxation without sacrificing sensitivity. Thermal Gravimetric Analysis (TGA) was carried out using Mettler Toledo TGA/DSC-1.

Conductivity measurements

The conductivity measurements were performed using Electrochemical Impedance Spectroscopy (EIS) employing a dip probe cell with two platinum foils in a glass casing, with a cell factor of 1.04 cm^{-1}. Impedance spectra were recorded in a frequency range of 1 Hz to 200 kHz with an amplitude of 25 mV. All the samples were first degassed with nitrogen flux and the

measurement was done under N_2 flux in a temperature range from 5 °C to 70 °C in a climatic chamber (Angelantoni). For all the samples, the bulk ohmic resistance was recorded via the x-axis intercept of high frequency side in the Nyquist plots.

Electrode/Cell Preparation

Prior to the use with aqueous electrolytes, the electrode materials (CLTP/LTP) were characterized in benchmark organic electrolytes. Slurries of active materials, PVDF (6020 by Solvay) binder and carbon black (Super P from Erachem Comilog, Inc.) in weight ratio 8:1:1 were prepared using anhydrous N-Methyl-2-Pyrrolidone (Merck) as the solvent. For the measurements in organic electrolytes, the slurries were casted on metal foils (Al) and R2032 coin cells were assembled in an argon-filled glovebox ($[O_2] < 0.1$ ppm, $[H_2O] < 0.1$ ppm) using alkaline metal foils (Li, Na, K) as the counter electrodes. The active material loads were ~2.4 mg cm^{-2}, ~2.7 mg cm^{-2} and ~1.7 mg cm^{-2} for Li, Na and K based cells, respectively. The cells were equipped with commercially available 1.0 M $LiPF_6$ in EC/DMC (LP30, Merck), 1 M $NaClO_4$ (Merck) in PC/FEC and 0.8 M KPF_6 (Merck) in EC/DEC to test the Li^+, Na^+ and K^+ intercalation, respectively. To avoid possible corrosion problems, the NASICON-based electrodes for aqueous electrolytes were prepared by dip-coating carbon cloth current collectors in the slurries of the active materials. In this case, the active material load was ~6 mg cm^{-2}.

Electrochemical Measurements

The ESW was estimated in flooded three-electrode cells equipped with glassy carbon as working, platinum mesh as counter and double junction SCE as reference electrode, respectively. Galvanostatic Charge-Discharge with Potential Limitation (GCPL) technique was used in the proper potential range at different current rates for the investigation of the performance of the NASICON/electrolytes interfaces. In the case of aqueous electrolytes, the GCPL measurement was

done using a flooded three-electrodes cell with a double junction SCE and a Pt foil as reference and counter electrodes, respectively.

All the GCPL measurements have been conducted at different current rates using the same protocol to compare the different interfaces, i.e. starting with 10 cycles at 0.1 C, then increasing the current every 10 cycles to 0.5 C, 1 C, 5C, and 10 C, and finally reducing the current again at 0.1 C for the last 10 cycles. In the C-rate calculation, 1C value corresponds to 136 mA g^{-1}, considering the insertion and de-insertion of two alkaline ions into the structure. To characterize the electrode electrolyte interface, EIS measurements were conducted in temperature range of 20 °C to 70 °C inside the climatic chamber. EIS spectra were recorded in a frequency range of 1 kHz to 100 KHz using a sinusoidal voltage of 50 mV under N_2 in a flooded cell, using three-electrode configuration. To avoid any interference from the surrounding, all the impedance measurements were carried out in a Faraday cage inside the climatic chamber.

Results and Discussion

Figure 1 reports the DSC thermograms of the electrolyte solutions. The samples show distinct thermal features which include the glass transition temperature (T_g) below -70 °C, exotherms of cold crystallization (T_c) below -20 °C, and finally the melting endotherms (T_m) around 0 C°. It can be observed that increasing the salt concentration result in the shifting of T_g to higher temperatures (see Table 2) which is correlated to a growing interaction among the solution species. Such increase in the T_g with concentration accounts for the transition of the solution characteristics from salt-in-water to water-in-salt as already reported for KAc solutions [17] and LiTFSI [24]. The T_g of all the samples showed an overshot which can be ascribed to structural relation [25]. Interestingly, 1N20K and 2.5N20K did not show any cold crystallization, or melting endotherm, meaning that they were frozen in the glassy state with the employed thermal protocol. In the case of 5N20K and

7N20K, single cold crystallization events occurred at -28.06 °C and -33.70 °C, respectively, while melting endotherms were recorded for both these samples at around 0 °C. However, the shape of the endotherms suggests that the melting process started well below the room temperature. Reber et al. [26] reported liquidus temperatures for similar electrolytes such as 35 mol kg^{-1} NaFSI, 30 mol kg^{-1} NaFSI with 5 mol kg^{-1} NaFTFSI, 25 mol kg^{-1} NaFSI with 10 mol kg^{-1} NaFTFSI, and 19.5 mol kg^{-1} LiTFSI with 8.3 mol kg^{-1} LiBETI, equal to 50 °C, 44 °C, 38 °C and 28 °C, respectively. They also reported liquidus temperatures of 28 °C and 22 °C for 35 mol kg^{-1} LiFSI and for 25 mol kg^{-1} LiFSI with 10 mol kg^{-1} LiFTFSI, respectively [26]. It is thus evident that even using different anions by mixing FSI and FTFSI didn't influence the liquidus temperature to a great extent. In this scenario, our electrolyte 7N20K will provide a significant advantage by preventing premature cell failure caused by salt crystallization in long-term cycling.

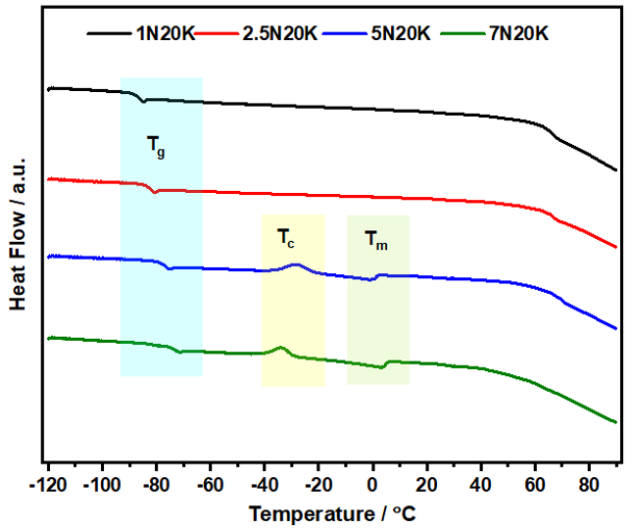

Figure 1. DSC curves of electrolytes (ENDO direction bottom). Concentration increases from top to bottom

The dependence of ionic conductivity on temperature for different concentrations is displayed in Figure 2a. Even in the relatively narrow temperature range we explored, all the compositions follow Vogel-Tamman-Fulcher'' (VTF) behavior [6]:

$$\sigma = \sigma_o \exp\left(\frac{-B}{T-To}\right) \quad (1)$$

Here B is a pseudo-activation energy for ions transport (E_a=$k_B B$), T is the absolute temperature and T_o can be interpreted as the ideal glass transition temperature.

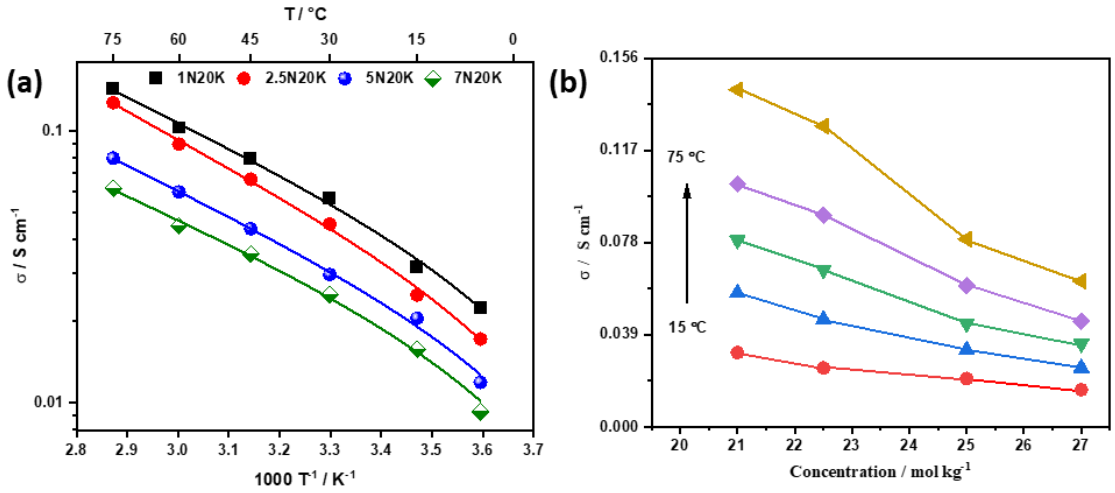

Figure 2. (a) Arrhenius plot of ionic conductivity. Continuous lines correspond to VTF best-fits with values of R^2>0.99; **(b)** conductivity values vs. total salt concentration at different temperatures (15 °C to 75 °C ,ΔT= 15 °C)

The ionic conductivity decreases with increasing the electrolyte concentration (Figure 2b), as expected in highly concentrated electrolytes. All the sodium containing samples, indeed, show values lower or nearly equal to that of 20 m CH_3COOK[17], however the 7N20K concentration still exhibits a good value of conductivity i.e., 21.2 mS cm^{-1} at 25°C (see Table 2). The decrease in ionic conductivities with increasing salt concentration is related to the T_g shift to higher temperatures, which determines the increase of viscosity resulting in increased resistance to the

shear flow [27,28]. The values of T_o are in good agreement with values of T_g from DSC measurements (see Table 2) and the two temperatures have the same dependence on concentration. An increase in concentration is associated with high T_o values as a result of a higher activation barrier to the movement of ions [29]. This dependence of T_o on concentration is attributed to the strong interaction between the ions and water molecules suggesting the formation of an internal liquid structure. The considerable levels of conductivity at high concentration strongly suggest the possibility of the formation of water-salt structures [27]. Here, the available water molecules cannot effectively shell the respective cations, promoting the interaction of anions (CH_3COO^- in our case) with the cations without causing any significant reassociation resulting in the modification of the local hydrogen bonding [30]. The molar conductivities (Λ_m), activation energies (E_a), ionic conductivities (σ), T_o and T_g values are reported in Table 2.

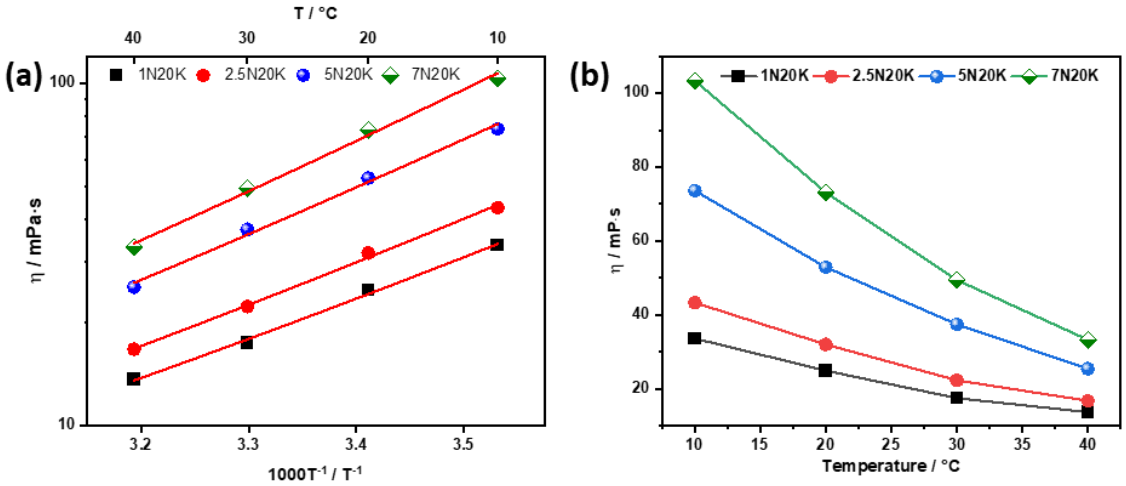

Figure 3. **(a)** Arrhenius plot of viscosity. The dashed lines show linear regression with $R^2 > 0.99$. **(b)** Viscosity of all samples vs. temperature

The results on the charge transport are supported also by the viscosity measurements vs. the temperatures, which follow an Arrhenius behavior (Figure 3a) for all the electrolyte samples. As

expected, the viscosities increase as a function of concentration, however, the trend does not vary linearly as it is in the case of diluted solutions (Stokes-Einstein equation) due to complex ion interactions at elevated concentrations [31]. In the case of salts having a similar anion (as in our case) the change in viscosity is predominantly caused by the cations [32]. Moreover, the behavior of aqueous concentrated acetates renders them as the so-called "structure-making salts'', because none of the samples show any decrease in viscosity with increasing salt concentration. Furthermore, this behavior signifies the reduced activity of water molecules, since the cations and acetate anions being strongly hydrated are contributing to some fashion of molecular ordering [33].

Figure 3b shows the evolution of viscosity as a function of temperature. All the electrolyte samples behave like Newtonian fluids (see Supplementary Information, Figures S1-S4). The viscosity should follow the empirical VTF equation, however, in the limited temperature range we could explore due to instrumental limitations, nearly all the compositions followed a simple Arrhenius behavior:

$$\eta = \eta_o \exp\left(\frac{E_a}{k_B T}\right) \quad (2)$$

Here E_a is the activation energy that is related to ion-ion and ion-solvent interactions, while k_B is the Boltzmann constant. Table 2 reports the E_a values of the electrolytes calculated from the viscosity data. The activation energy increases with increasing the concentration and are in good agreement with the values of obtained from conductivity measurements, and also with the glass transition behavior. This confirms that the mechanisms at the base of bulk properties such as ionic transport and viscosity are well correlated.

Table 2. Conductivity values, activation energies calculated from viscosity and conductivity data.

Sample Name	Molarity (mol·dm^{-3})	E_a (η) (eV)	σ (25 °C) (mS cm^{-1})	Λ_m (25 °C) (S cm^2 mol^{-1})	E_a (σ) (eV)	T_o (K)	T_g (K)
1N20K	9.45	0.232	49.97	5.29	0.262	217	185

2.5N20K	9.87	0.245	41.13	4.16	0.270	219	189
5N20K	10.38	0.269	29.75	2.87	0.273	222	194
7N20K	10.76	0.289	21.21	1.97	0.296	228	197

$E_a(\eta)$ = activation energy from viscosity, σ = specific conductivity, Λ_m = molar conductivity, $E_a(\sigma)$ = activation energy from conductivity, T_o = Vanishing mobility temperature

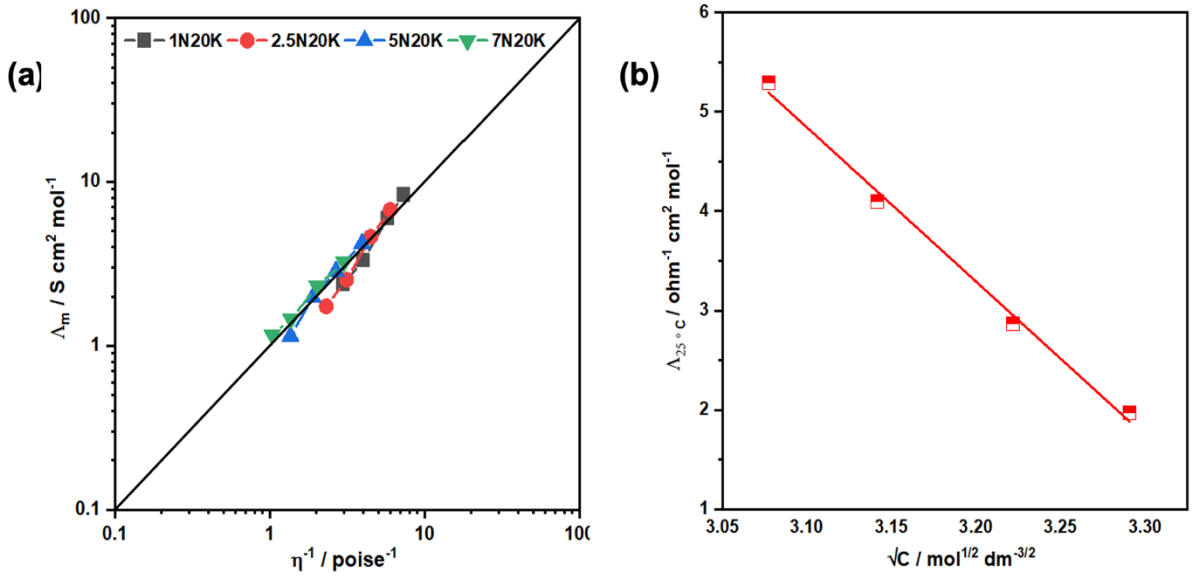

Figure 4. (a) Walden Plot for acetate solutions. The straight line indicates the behavior of KCl as a reference. **(b)** Plot of molar conductivity vs. square root of concentration.

Since viscosity is inversely related to molar conductivity, the classical Walden plot can be used to probe the ionicity of the acetate electrolytes. Figure 4a shows the molar/conductivities vs. the fluidity η^{-1} at different temperatures. The straight line is the ideal line for completely dissociated ionic systems, e.g., KCl diluted aqueous solutions. The degree of fluidity of the medium is directly related to the association of ions in the electrolyte solutions [34]. According to Figure 4a, all the electrolytes can be classified as quasi-ideal electrolytes [35,36]. As expected, the higher the temperature, the better the ideality. The most concentrated solution 7N20K, which is of particular interest in Na ion batteries, follows Kohlrausch's law of strong electrolytes, as reported in Figure 4b for the values at 25 °C:

$$\Lambda_m = \Lambda_o - Ac^{1/2} \quad (3)$$

where Λ_o is the molar conductivity at infinite dilution, A is a constant depending on the composition and stoichiometry of the solution, and c represents the molarity. At 25 °C, Λ_o has a value of 52.90 ohm^{-1} cm^2 mol^{-1}. Thus, even at the highest possible concentrations, the Kohlrausch law calls for complete salt dissociation [37].

Figure 5 shows the linear sweep voltammetry (LSV) profiles vs standard hydrogen electrode (SHE) for the electrolyte samples. For the estimation of decomposition potentials of water, a threshold of 0.1 mA cm^{-2} is taken as a limit on the glassy carbon electrode. The present procedure may lead to overestimated decomposition limits because it involves a large amount of electrolyte and a quasi-ideal electrocatalytic electrode with a small surface area. However, it has the advantages of being highly reproducible and it is useful to evaluate and compare different electrolytes.

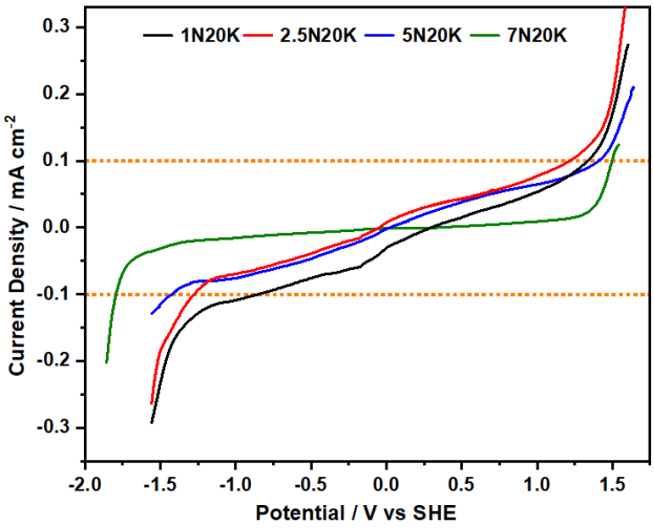

Figure 5. Electrochemical stability window of water vs SHE

The cathodic and anodic decomposition potentials for all the samples obtained in these conditions are summarized in Table 3. The noticeable increase in the stability on the cathodic side

with increasing salt concentration confirms an obvious suppression of the hydrogen evolution. This is a confirmation for the reduced activity of water in agreement with the rheological and thermal analysis. The ESW expansion on the anodic side is not as significant as it is on the cathodic one, in agreement with previously reported results on acetate-based electrolytes [17].

Table 3. Cathodic and Anodic stability limits, ESW

Sample Name	Cathodic Limit (V)	Anodic Limit (V)	Estimated ESW (V)
1N20K	-0.84	1.33	2.17
2.5N20K	-1.27	1.21	2.48
5N20K	-1.42	1.40	2.82
7N20K	-1.79	1.49	3.28

Thanks to the good conductivity, broad ESW of WISE, and the large concentration of alkaline cations, the 7N20K was coupled with a NASICON $LiTi_2(PO_4)_3$ based electrode to study an anodic interface for alkaline ion battery. As already demonstrated in the literature, the low electrical conductivity of this NASICON phase requires a carbon shell around the active material particles to enable good electrochemical performances [23]. Following this approach, the coated NASICON (CLTP) was produced by one pot sol gel route in presence of a carbonaceous precursor (glucose). For sake of comparison, the same synthesis was repeated in absence of glucose, obtaining the pristine $LiTi_2(PO_4)_3$ material (LTP).

The XRD patterns of the LTP and CLTP samples are reported in Supporting Information (Figure S5) and show the phase purity without crystalline secondary phases. All the peaks are indeed in good agreement with the rhombohedral NASICON type crystal structure (R-3c space group, JCPDS: 35-0754) [38]. The peak positions in both samples are the same, signifying that the carbon content present in the coated sample does not affect the crystal structure, which consists of

$[Ti_2(PO_4)_3]^-$ framework built by a (PO_4) tetrahedral and a corner-sharing (TiO_6) octahedral. Interstitial sites which can accommodate a variety of ions are created by the linking of three (PO_4) tetrahedra and two (TiO_6) octahedra along the c-axis [39]. The morphological properties of both powders were observed by SEM. The sol gel route produces irregular porous particles in the micrometric range, with size around 10/15 μm, and a very irregular surface morphology (Figure S6 in the SI). When the glucose is added during the synthesis, the resulting LTP particles surface is covered with a layer of carbon nanoparticles, which are beneficial for the electron distribution through the composite electrode. The carbon content in the CLTP is around 4.20 % as confirmed by TGA analysis (see Figure S7 in SI).

The electrochemical performances of CLTP and LTP at different currents were first tested in organic electrodes, building half cells vs. metallic Li, Na, and K, respectively. The results, reported in Figure S8 and S9 in the Supporting Information, demonstrated the need for intimate carbon/active material contact. The CLTP based-electrode, indeed, outperforms LTP in the Li based electrolyte and shows a first cycle specific capacity of 129, 113, and 92 mAh g^{-1} in LiPF6, $NaPF_6$, and KPF_6 (Figure S8), respectively which are close to the theoretical value for the insertion of two alkaline ions (138 mAh g^{-1}) in the structure. The electrochemical data obtained in the organic electrolytes are summarized in table S2 of the SI.

A direct comparison among the potential profiles in the different organic electrolytes is also very useful to understand the mechanism of the ion insertion in solutions containing more cationic species. In Figure 6, the first cycles in the three electrolytes are reported using both the Li^+/Li and the SHE reference electrode scale. As it is possible to observe, apart from differences in the specific capacity, Li^+ and Na^+ have insertion potentials that are quite close and comparable, while the insertion of potassium into the structure needs an extra reducing potential of about 0.9 V, probably

because of the higher energy required to introduce and accommodate the larger K^+ ion into the crystalline structure. This suggest that in a Na^+/K^+ mixed electrolyte, the Na^+ ions will be preferentially introduced in the anode.

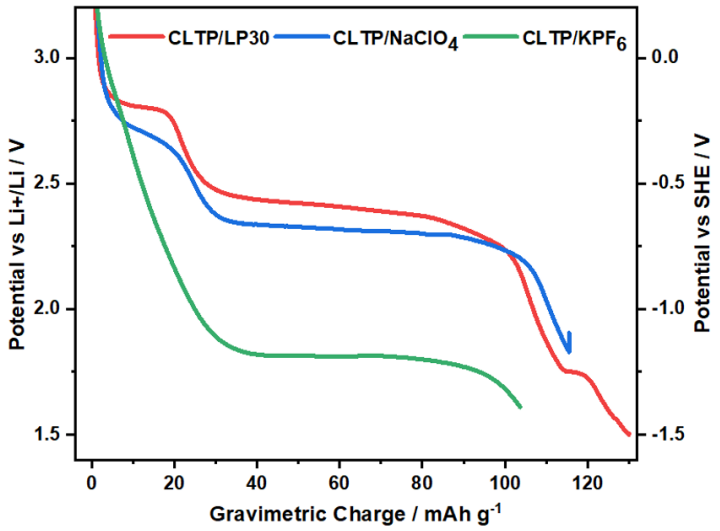

Figure 6. Alkaline ion insertion into CLTP in different organic electrolytes reported vs. the Li^+/Li (left) and the SHE (right) standard electrode potentials

The performance of CLTP was then evaluated in the 7N20K solution, for sake of comparison and to highlight the beneficial effect of the WISE approach, we have also tested the same electrode in 1 M NaAc aqueous electrolyte (Figure 7a and 7b). The potential profiles reported in Figure 7a show the preferential insertion of sodium cation as expected, despite its concentration being 2.85 times lower than that of potassium for 7N20K. Furthermore, Figure 7 also demonstrates that the performances in the WISE electrolyte are clearly better than those in the diluted solution in terms of specific capacity and efficiency. In particular, the cathodic and anodic capacities are 104 and 84 mAh g^{-1}, (80% charge efficiency) at the first cycle in 7N20K, while in the diluted solution the values decrease to 96 and 36 mAh g^{-1} (40% efficiency), respectively. Moreover, when cycled in the WISE electrolyte at 1C (136 mA g^{-1}) the CLTP is capable to provide an average anodic specific

capacity of 68 mAh g^{-1} with an average charge efficiency of 99.0%. Finally, at the end of the test (60 cycles), the CLTP/WISE interface shows a capacity retention of 90%.

To better understand the electrode/electrolyte interface, the kinetics of the mechanism of charge transfer, and the diffusion of alkaline ions inside the electrode structure, EIS analysis was performed on a partially sodiated CLTP electrode. To do so CLTP was first sodiated while during the de-sodiation the measurement was interrupted in the middle of the first plateau and EIS spectra were collected at every 10 °C steps from 20 °C to 70 °C. As shown in Figure 8, all the impedance spectra exhibit similar shape: a depressed semicircle followed by a straight line related to the Warburg element.

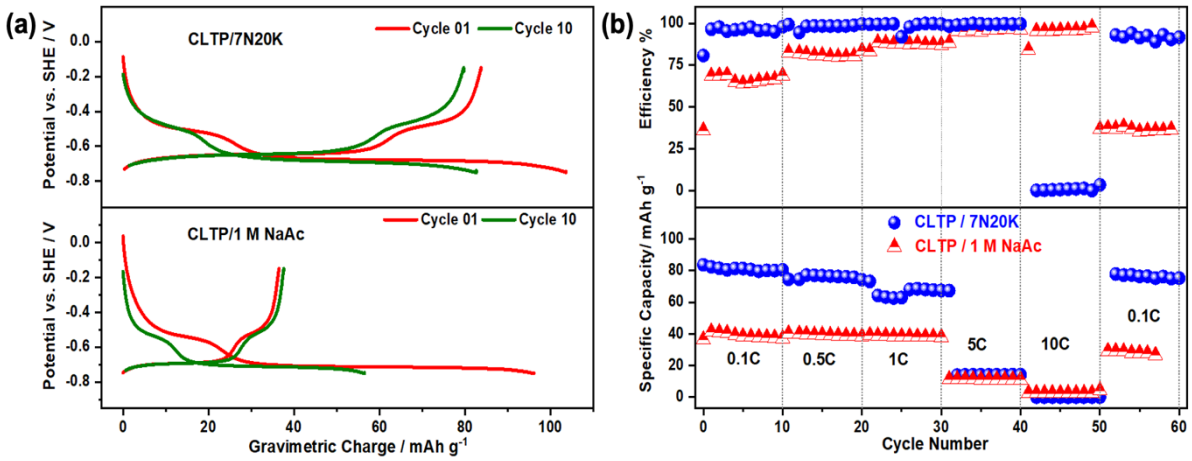

Figure 7. (a) GCPL curves of CLTP in aqueous electrolytes **(b)** rate performance in CLTP in aqueous electrolytes

The charge transfer resistance was evaluated as the intercept of the linear part of the impedance with the x-axis (real part of the impedance) and subtracting the electrolyte contribution, i.e. the high frequency intercept of the charge transfer arc. The activation energy of the charge transfer was calculated using the empirical Arrhenius equation:

$$R_{CT}(T) = R_{CT,inf} e^{\frac{E_a}{k_B T}} \quad (4)$$

where $R_{CT,inf}$ is the charge transfer resistance at infinite temperature, and E_a the activation energy. Figure 9 shows the Arrhenius plot of the charge transfer resistance. The low activation energy (0.12 eV) proves the very good kinetic properties of the interface between the NASICON electrode and the highly concentrated electrolyte.

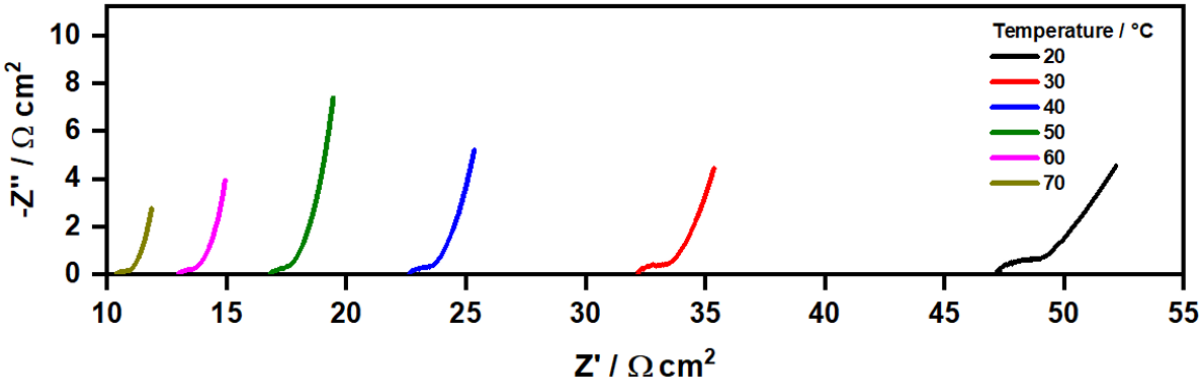

Figure 8. Electrochemical impedance spectra of CLTP at different temperatures in 7N20K

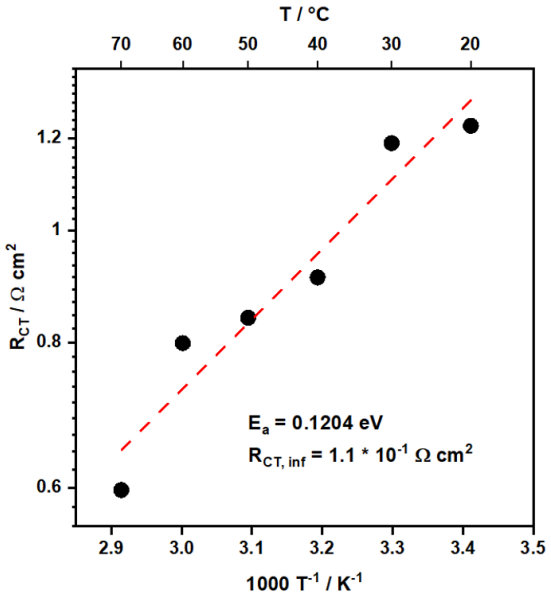

Figure 9. Arrhenius plot of charge transfer resistance of CLTP in 7N20K

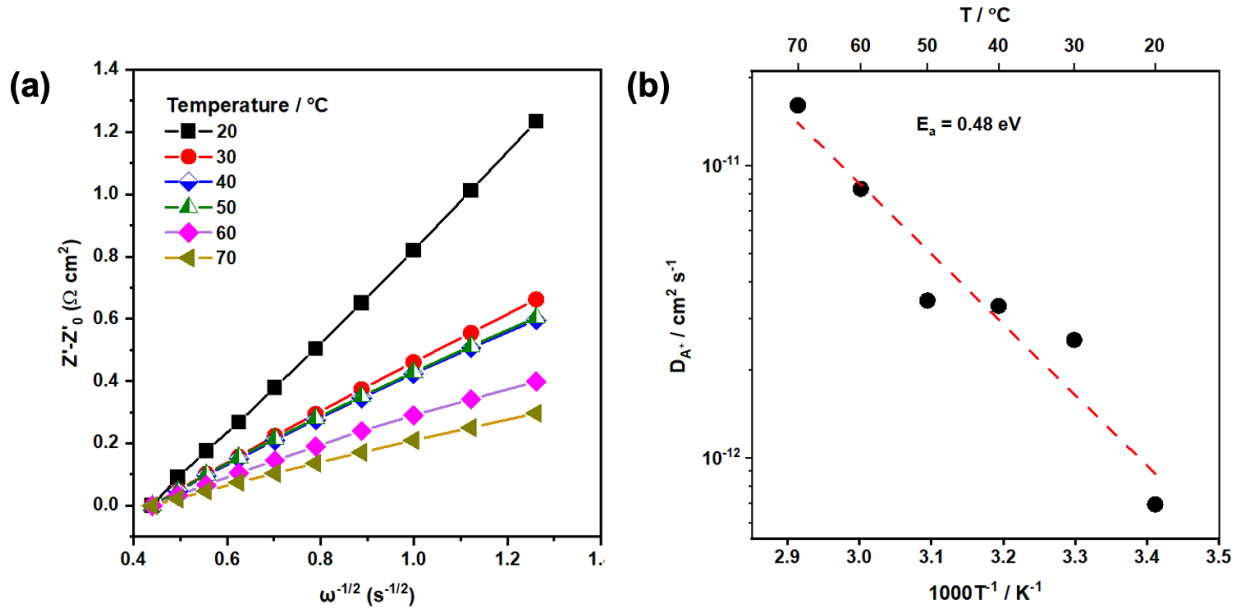

Figure 10. (a) Evaluation of the diffusion coefficient of alkaline ions (lithium and sodium) inside LTP structure. Linear relationship between Z' and $\omega^{-\frac{1}{2}}$ in the diffusion-controlled region of the impedance (low frequencies). **(b)** Arrhenius plot of the diffusion coefficient

The diffusion coefficient is calculated via the following formula:

$$D_{A^+} = \left(\frac{RT}{\sqrt{2}\,An^2F^2C\sigma_W}\right)^2 \tag{5}$$

where R is the gas constant, T is the absolute temperature, A is the surface area of the electrode, n is the number of mobile ions inside the structure (evaluated to be 1.7 in the case of the impedance measurements), F is the Faraday's constant ($96485\ C\ mol^{-1}$), C is the concentration of the mobile ions inside the electrode structure (volume considered to be constant, concentration value $12930\ mol\ m^{-3}$) and σ_W is the Warburg coefficient. Figure 10 (a) shows the linear relationship between the real part of the impedance and $\omega^{-\frac{1}{2}}$. The slope of the lines is in fact the Warburg coefficient, which is used in the previous formula to obtain the diffusion coefficient. As shown in Figure (b) the diffusion coefficient follows the Arrhenius relationship:

$$D_{A^+}(T) = D_{A^+,inf}\, e^{-\frac{E_a}{k_B T}} \quad (6)$$

The value of the diffusion coefficient 'D' at room temperature (around $10^{-13}\ cm^2\ s^{-1}$) is in line with other reports in the literature[40]. Also, it is noteworthy that the aqueous electrolyte improves the diffusion of alkaline-ions inside the electrode structure, as previously reported [41]. Moreover, the low activation energy value (0.48 eV) suggests that the diffusion can be easily improved by increasing the temperature.

Conclusions

In this work, the physico-chemical properties of a series of binary aqueous acetate salts solutions are thoroughly investigated via DSC, rheological, electrical, and electrochemical measurements. Four different solutions are prepared by dissolving 20 mol kg^{-1} of CH_3COOK, with different amounts of CH_3COONa, ranging from 1 to 7 mol kg^{-1}. DSC analysis carried out in a temperature range of -120 °C to 90 °C revealed that the glass transition temperature T_g increases with increasing the salt concentration. Moreover, the DSC also confirms the low liquidus temperature for the 7N20K sample. Viscosity measurements carried out as a function of temperature classified the acetate salts to be the so-called ''structure making salts''. The ionic conductivity decreased by increasing the salt concentration, however, it remained comparable to the organic counterparts even for the highest concentration (21.2 mS cm^{-1} at 25°C for 7N20K). Electrochemical measurements carried out in ideal conditions showed that the electrochemical stability window increased by increasing the CH_3CCONa concentration. To test the possible use in alkaline ion batteries, a carbon-coated NASICON based electrode was used as an anode. The performances were quite promising, with a first cycle anodic capacity of 85 mAh g^{-1}, an average charge efficiency of 96% and 99% at low and high currents, respectively, and a 90% capacity retention after 60 cycles. Moreover, the impedance spectroscopy measurements performed as a function of

the temperature highlighted the very good kinetic properties of the NASICON/7N20K interface. These results demonstrated the possibility to design electrode interfaces for the successful development of alkaline ion rechargeable batteries in the context of the water-in-salt approach.

ASSOCIATED CONTENT

Supporting Information.

The following files are available free of charge.

Shear stress vs shear rate curves for the aqueous electrolytes; XRPD patters, SEM images and thermal analysis for the NASICONs, additional electrochemical characterization of the NASICONs in the organic electrolytes.

Corresponding Author

Email: riccardo.ruffo@unimib.it

Author Contributions

S.K. and N.P. led the investigations and the data curation, S.B. contributed to investigations and data curations. S.K. R.R., P.M. led the conceptualization, the methodology and supervised the investigations, N.P. contributed to the methodology, S.K., R.R. and P.M: led the writing, all authors contributed to the review and editing in equal manner. All authors have given approval to the final version of the manuscript.

Funding Sources

This work has been financed by: Ministry of University and Research (MIUR) through grant “Dipartimenti di Eccellenza - 2017 “Materials for Energy”..

Notes

The authors declare no competing financial interest

ABBREVIATIONS

NASICON, Na super ionic conductor, LiBs, Lithium ion batteries, ESW, electrochemical stability window, sodium acetate, NaAc, potassium acetate, KAc, $LiTi_2(PO_4)$, LTP, Carbon-coated $LiTi_2(PO_4)_3$ (CLTP)

REFERENCES

(1) Borodin, O.; Self, J.; Persson, K. A.; Wang, C.; Xu, K. Uncharted Waters: Super-Concentrated Electrolytes. *Joule*. Cell Press January 15, 2020, pp 69–100. https://doi.org/10.1016/j.joule.2019.12.007.

(2) Mauger, A.; Julien, C. M. Critical Review on Lithium-Ion Batteries: Are They Safe? Sustainable? https://doi.org/10.1007/s11581-017-2177-8.

(3) Reza Younesi, L.-S.; Gabriel Veith, ab M.; Johansson, P.; Kristina Edströ be, de; Vegge, T. Lithium Salts for Advanced Lithium Batteries. *Cite this Energy Environ. Sci* **2015**, *8*, 1905. https://doi.org/10.1039/c5ee01215e.

(4) Droguet, L.; Grimaud, A.; Fontaine, O.; Tarascon, J. M. Water-in-Salt Electrolyte (WiSE) for Aqueous Batteries: A Long Way to Practicality. *Adv. Energy Mater.* **2020**, *10* (43), 2002440. https://doi.org/10.1002/aenm.202002440.

(5) McKinnon, W. R.; Dahn, J. R. How to Reduce the Cointercalation of Propylene Carbonate in Li and Other Layered Compounds. *J. Electrochem. Soc.* **1985**, *132* (2), 364. https://doi.org/10.1149/1.2113839.

(6) Quartarone, E.; Mustarelli, P. Electrolytes for Solid-State Lithium Rechargeable Batteries: Recent Advances and Perspectives. *Chem. Soc. Rev.* **2011**, *40* (5), 2525–2540.

https://doi.org/10.1039/C0CS00081G.

(7) Suo, L.; Hu, Y. S.; Li, H.; Armand, M.; Chen, L. A New Class of Solvent-in-Salt Electrolyte for High-Energy Rechargeable Metallic Lithium Batteries. *Nat. Commun.* **2013**, *4*. https://doi.org/10.1038/ncomms2513.

(8) R. Lukatskaya, M.; I. Feldblyum, J.; G. Mackanic, D.; Franziska Lissel; L. Michels, D.; Yi Cui; Zhenan Bao. Concentrated Mixed Cation Acetate "Water-in-Salt" Solutions as Green and Low-Cost High Voltage Electrolytes for Aqueous Batteries. *Energy Environ. Sci.* **2018**, *11* (10), 2876–2883. https://doi.org/10.1039/C8EE00833G.

(9) Miyazaki, K.; Takenaka, N.; Watanabe, E.; Iizuka, S.; Yamada, Y.; Tateyama, Y.; Yamada, A. First-Principles Study on the Peculiar Water Environment in a Hydrate-Melt Electrolyte. *J. Phys. Chem. Lett.* **2019**, *10* (20), 6301–6305. https://doi.org/10.1021/ACS.JPCLETT.9B02207.

(10) Reber, D.; Grissa, R.; Becker, M.; Kühnel, R.-S.; Battaglia, C. Anion Selection Criteria for Water-in-Salt Electrolytes. *Adv. Energy Mater.* **2021**, *11* (5), 2002913. https://doi.org/10.1002/AENM.202002913.

(11) Suo, L.; Borodin, O.; Gao, T.; Olguin, M.; Ho, J.; Fan, X.; Luo, C.; Wang, C.; Xu, K. *"Water-in-Salt" Electrolyte Enables High-Voltage Aqueous Lithium-Ion Chemistries*.

(12) Suo, L.; Borodin, O.; Wang, Y.; Rong, X.; Sun, W.; Fan, X.; Xu, S.; Schroeder, M. A.; Cresce, A. V.; Wang, F.; Yang, C.; Hu, Y. S.; Xu, K.; Wang, C. "Water-in-Salt" Electrolyte Makes Aqueous Sodium-Ion Battery Safe, Green, and Long-Lasting. *Adv. Energy Mater.* **2017**, *7* (21). https://doi.org/10.1002/aenm.201701189.

(13) Ku, R.-S.; Reber, D.; Battaglia, C. A High-Voltage Aqueous Electrolyte for Sodium-Ion Batteries. **2017**, *2*, 53. https://doi.org/10.1021/acsenergylett.7b00623.

(14) Jiang, L.; Lu, Y.; Zhao, C.; Liu, L.; Zhang, J.; Zhang, Q.; Shen, X.; Zhao, J.; Yu, X.; Li, H.; Huang, X.; Chen, L.; Hu, Y.-S. Building Aqueous K-Ion Batteries for Energy Storage. *Nat. Energy* **2019**, *4*. https://doi.org/10.1038/s41560-019-0388-0.

(15) Yang, C.; Chen, J.; Qing, T.; Fan, X.; Sun, W.; Cresce, A. von; Ding, M. S.; Borodin, O.; Vatamanu, J.; Schroeder, M. A.; Eidson, N.; Wang, C.; Xu, K. 4.0 V Aqueous Li-Ion Batteries. *Joule* **2017**, *1* (1), 122–132. https://doi.org/10.1016/J.JOULE.2017.08.009.

(16) Yongqi Deng; Hongfei Wang; Kefu Zhang; Jingwen Shao; Jun Qiu; Juan Wu; Yihan Wu; Lifeng Yan. A High-Voltage Quasi-Solid-State Flexible Supercapacitor with a Wide Operational Temperature Range Based on a Low-Cost "Water-in-Salt" Hydrogel Electrolyte. *Nanoscale* **2021**, *13* (5), 3010–3018. https://doi.org/10.1039/D0NR08437A.

(17) Stigliano, P. L.; Pianta, N.; Bonizzoni, S.; Mauri, M.; Simonutti, R.; Lorenzi, R.; Vigani, B.; Berbenni, V.; Rossi, S.; Mustarelli, P.; Ruffo, R. A Physico-Chemical Investigation of Highly Concentrated Potassium Acetate Solutions towards Applications in Electrochemistry. *Phys. Chem. Chem. Phys.* **2021**, *23* (2), 1139–1145. https://doi.org/10.1039/d0cp04151c.

(18) Tribbia, M.; Pianta, N.; Brugnetti, G.; Lorenzi, R.; Ruffo, R. A New Double Layer Super-Capacitor Made by Free-Standing Activated Carbon Membranes and Highly Concentrated Potassium Acetate Solutions. *Electrochim. Acta* **2020**, *364*, 137323. https://doi.org/10.1016/J.ELECTACTA.2020.137323.

(19) Leonard, D. P.; Wei, Z.; Chen, G.; Du, F.; Ji, X. Water-in-Salt Electrolyte for Potassium-Ion Batteries. *ACS Energy Lett.* **2018**, *3* (2), 373–374. https://doi.org/10.1021/ACSENERGYLETT.8B00009.

(20) Chen, S.; Lan, R.; Humphreys, J.; Tao, S. Salt-Concentrated Acetate Electrolytes for a High Voltage Aqueous Zn/MnO2 Battery. *Energy Storage Mater.* **2020**, *28*, 205–215. https://doi.org/10.1016/J.ENSM.2020.03.011.

(21) Chen, S.; Wu, C.; Shen, L.; Zhu, C.; Huang, Y.; Xi, K.; Maier, J.; Yu, Y. Challenges and Perspectives for NASICON-Type Electrode Materials for Advanced Sodium-Ion Batteries. *Adv. Mater.* **2017**, *29* (48), 1700431. https://doi.org/10.1002/ADMA.201700431.

(22) Han, J.; Zarrabeitia, M.; Mariani, A.; Jusys, Z.; Hekmatfar, M.; Zhang, H.; Geiger, D.; Kaiser, U.; Behm, R. J.; Varzi, A.; Passerini, S. Halide-Free Water-in-Salt Electrolytes for

Stable Aqueous Sodium-Ion Batteries. *Nano Energy* **2020**, *77* (May), 105176. https://doi.org/10.1016/j.nanoen.2020.105176.

(23) Wessells, C.; La Mantia, F.; Deshazer, H.; Huggins, R. A.; Cui, Y. Synthesis and Electrochemical Performance of a Lithium Titanium Phosphate Anode for Aqueous Lithium-Ion Batteries. *J. Electrochem. Soc.* **2011**, *158* (3), A352. https://doi.org/10.1149/1.3536619/XML.

(24) Suo, L.; Hu, Y.-S.; Li, H.; Armand, M.; Chen, L. A New Class of Solvent-in-Salt Electrolyte for High-Energy Rechargeable Metallic Lithium Batteries. *Nat. Commun. 2013 41* **2013**, *4* (1), 1–9. https://doi.org/10.1038/ncomms2513.

(25) Mustarelli, P.; Tomasi, C. Heat Capacities of Thermally Treated Na2O-3B2O3 Glasses Above and Below Tg. *Zeitschrift für Naturforsch. A* **1996**, *51* (3), 187–191. https://doi.org/10.1515/ZNA-1996-0309.

(26) Reber, D.; Ku, R.-S.; Battaglia, C. Suppressing Crystallization of Water-in-Salt Electrolytes by Asymmetric Anions Enables Low-Temperature Operation of High-Voltage Aqueous Batteries. **2021**, *14*, 26. https://doi.org/10.1021/acsmaterialslett.9b00043.

(27) Ding, M. S.; Cresce, A. von; Xu, K. Conductivity, Viscosity, and Their Correlation of a Super-Concentrated Aqueous Electrolyte. *J. Phys. Chem. C* **2017**, *121* (4), 2149–2153. https://doi.org/10.1021/ACS.JPCC.6B12636.

(28) Ding, M. S. Conductivity and Viscosity of PC-DEC and PC-EC Solutions of LiBF4. *J. Electrochem. Soc.* **2003**, *151* (1), A40. https://doi.org/10.1149/1.1630593.

(29) Gu, G. Y.; Bouvier, S.; Wu, C.; Laura, R.; Rzeznik, M.; Abraham, K. M. 2-Methoxyethyl (Methyl) Carbonate-Based Electrolytes for Li-Ion Batteries. *Electrochim. Acta* **2000**, *45* (19), 3127–3139. https://doi.org/10.1016/S0013-4686(00)00394-7.

(30) Lukatskaya, M. R.; Feldblyum, J. I.; Mackanic, D. G.; Lissel, F.; Michels, D. L.; Cui, Y.; Bao, Z. Concentrated Mixed Cation Acetate "Water-in-Salt" Solutions as Green and Low-Cost High Voltage Electrolytes for Aqueous Batteries. *Energy Environ. Sci.* **2018**, *11* (10), 2876–2883. https://doi.org/10.1039/c8ee00833g.

(31) El Halimi, M. S.; Poli, F.; Mancuso, N.; Olivieri, A.; Mattioli, E. J.; Calvaresi, M.; Chafik, T.; Zanelli, A.; Soavi, F. Circumneutral Concentrated Ammonium Acetate Solution as Water-in-Salt Electrolyte. *Electrochim. Acta* **2021**, *389*, 138653. https://doi.org/10.1016/J.ELECTACTA.2021.138653.

(32) Hao Du, †; Jayendran C. Rasaiah, ‡ and; Jan D. Miller*, †. Structural and Dynamic Properties of Concentrated Alkali Halide Solutions: A Molecular Dynamics Simulation Study. *J. Phys. Chem. B* **2006**, *111* (1), 209–217. https://doi.org/10.1021/JP064659O.

(33) Peng, H.; Nguyen, A. V. A Link between Viscosity and Cation-Anion Contact Pairs: Adventure on the Concept of Structure-Making/Breaking for Concentrated Salt Solutions. *J. Mol. Liq.* **2018**, *263*, 109–117. https://doi.org/10.1016/J.MOLLIQ.2018.04.145.

(34) Angell, C. A.; Younes Ansari; Zuofeng Zhao. Ionic Liquids: Past, Present and Future. *Faraday Discuss.* **2011**, *154* (0), 9–27. https://doi.org/10.1039/C1FD00112D.

(35) Porion, P.; Dougassa, Y. R.; Tessier, C.; El Ouatani, L.; Jacquemin, J.; Anouti, M. Comparative Study on Transport Properties for LiFAP and LiPF6 in Alkyl-Carbonates as Electrolytes through Conductivity, Viscosity and NMR Self-Diffusion Measurements. *Electrochim. Acta* **2013**, *114*, 95–104. https://doi.org/10.1016/J.ELECTACTA.2013.10.015.

(36) Schreiner, C.; Zugmann, S.; Hartl, R.; Gores, H. J. Fractional Walden Rule for Ionic Liquids: Examples from Recent Measurements and a Critique of the So-Called Ideal KCl Line for the Walden Plot†. *J. Chem. Eng. Data* **2009**, *55* (5), 1784–1788. https://doi.org/10.1021/JE900878J.

(37) Fiegenbaum, F.; Peres, G.; De Souza, M. O.; Martini, E. M. A.; De Souza, R. F. Physicochemical Characterisation of Aqueous Solutions of Tetra-Alkyl-Ammonium-Sulfonic Acid Ionic Liquid. *J. Mol. Liq.* **2016**, *215*, 302–307. https://doi.org/10.1016/J.MOLLIQ.2015.12.046.

(38) Liu, L.; Zhou, M.; Wang, G.; Guo, H.; Tian, F.; Wang, X. Synthesis and Characterization of LiTi2(PO4)3/C Nanocomposite as Lithium Intercalation Electrode Materials.

Electrochim. Acta **2012**, *70*, 136–141. https://doi.org/10.1016/J.ELECTACTA.2012.03.046.

(39) Cui, Y.; Hao, Y.; Bao, W.; Shi, Y.; Zhuang, Q.; Qiang, Y. Synthesis and Electrochemical Behavior of LiTi2(PO4)3 as Anode Materials for Aqueous Rechargeable Lithium Batteries. *J. Electrochem. Soc.* **2012**, *160* (1), A53. https://doi.org/10.1149/2.060301JES.

(40) Sun, J.; Sun, Y.; Gai, L.; Jiang, H.; Tian, Y. Carbon-Coated Mesoporous LiTi2(PO4)3 Nanocrystals with Superior Performance for Lithium-Ion Batteries. *Electrochim. Acta* **2016**, *200*, 66–74. https://doi.org/10.1016/J.ELECTACTA.2016.03.071.

(41) Kim, D. J.; Ponraj, R.; Kannan, A. G.; Lee, H. W.; Fathi, R.; Ruffo, R.; Mari, C. M.; Kim, D. K. Diffusion Behavior of Sodium Ions in Na0.44MnO2 in Aqueous and Non-Aqueous Electrolytes. *J. Power Sources* **2013**, *244*, 758–763. https://doi.org/10.1016/j.jpowsour.2013.02.090.